Supplementary Information for

Akt phosphorylation of neuronal nitric oxide synthase regulates gastrointestinal motility in mouse ileum

Damian D. Guerra, Rachael Bok, Vibhuti Vyas, David J. Orlicky, Ramón A. Lorca, and K. Joseph Hurt

Corresponding author: K. Joseph Hurt
Email: K.Joseph.Hurt@ucdenver.edu

This PDF file includes:

Supplementary text
SI Appendix Figs. S1 to S13
SI Appendix Tables S1 to S2
References for SI reference citations

www.pnas.org/cgi/doi/10.1073/pnas.1905902116

Supplementary Materials

Animals

Ethics statement: The University of Colorado Institutional Animal Care and Use Committee approved all animal experiments and procedures (IACUC protocol 90).

Wildtype (WT): WT mice were C57Bl/6 from Charles River laboratories (Wilmington, MA) or genotyped WT siblings of nNOS^{S1412A} homozygotes.

eNOS KO: eNOS KO mice from the Jackson Laboratory (Bar Harbor, ME) stock 002684 are homozygous for the *NOS3*^{tm1Unc} allele. The *NOS3*^{tm1Unc} allele replaces 129bp of exon 12, which encodes the calmodulin (CaM) binding domain, with a premature stop codon (1).

nNOSα KO: nNOSα KO mice from the Jackson Laboratory stock 002986 are homozygous for the *NOS1*^{tm1Plh} allele. Since the *NOS1*^{tm1Plh} allele lacks the first nNOS exon, the resulting protein lacks amino acids 1-159 and no longer localizes to the plasma membrane (2, 3).

nNOS^{S1412A}: The nNOS^{S1412A} (S1412A) knock-in mouse contains a point mutation substituting nNOS serine-1412 with non-phosphorylatable alanine. We developed nNOS^{S1412A} mice with assistance from the CU Anschutz Transgenic and Gene Targeting Core.

We amplified a 6180 bp fragment containing *M. musculus* neuronal nitric oxide synthase (*nNOS/NOS1*) exons 27-29, and intervening introns (81,988-88,168bp downstream of the nNOS start codon), from BAC RP24-164C18 with primers containing 5` XhoI and ClaI sites and a 3` SpeI site. BAC RP24-164C18 contains bp 118,280,651-118,451,991 of *M. musculus* chromosome 5, which includes the entire *nNOS*

gene. We cloned the nNOS homology amplicon into a pBlueScript that lacked a NotI site by cutting both the vector and the amplicon with XhoI and SpeI, yielding pBS_nNOS.

We generated the nNOS^{S1412A} mutation by overlapping PCR: for the 5` PCR product (84,979-85,629bp downstream of the nNOS start codon), the forward primer contained an EcoRV site, and the reverse primer's 5` end encoded the Ser → Ala mutation (TCC→GCG). For the 3` PCR product (85,630-86,659bp downstream of nNOS start codon), the forward primer's 5` end contained the first nucleotide after the mutation, and the reverse primer contained a NotI site. We cut the resulting nNOS^{S1412A} overlap fragment and pBS_nNOS with EcoRV and NotI, and the nNOS^{S1412A} overlap fragment was cloned into the cut vector to yield pBS_nNOS(A). For positive and negative selectable markers, we added neomycin phosphotransferase flanked with loxP sites (LNL) and thymidine kinase (TK) to pBS_nNOS(A). The LNL contained 5` and 3` AflII sites and was cloned in the antisense orientation relative to the nNOS^{S1412A} overlap fragment between exons 27 and 28. The TK negative selection marker was cloned in the sense orientation downstream from the nNOS^{S1412A} overlap fragment.

We electroporated the ClaI-linearized targeting vector into mouse EC7.1 embryonic stem cells (mixed C57Bl/6 x 129 background), electroporated Cre (New England Biolabs; Ipswitch, MA) into G418-resistant cells to excise LNL cassettes, and karyotyped clones as before (4). We injected karyotypically normal clones into C57Bl/6 blastocysts, after which chimeric blastocysts were transferred into pseudopregnant C57Bl/6 mice to produce F0 chimeras. We genotyped chimeric progeny by three methods: 1. Primers specific to the excised neomycin resistance gene. 2. Primers specific to the remaining loxP site and adjoining nNOS sequence after successful Cre recombination. 3. A single nucleotide polymorphism Transnetyx (Cordova, TN) assay specific to the nNOS^{S1412A} mutation. nNOS^{S1412A} -positive and Neo^{R}-negative chimeras were crossed to C57Bl/6 mice (Charles River laboratories). We identified non-chimeric *nNOS^{S1412A}* heterozygotes by genotyping method 3 and backcrossed male heterozygotes to C57Bl/6 females. We further purified genetic backgrounds by crossing nNOS^{S1412A} heterozygous females

to C57Bl/6 males to replace the EC7.1 cell-inherited Y chromosome. All nNOS^{S1412A} homozygotes (Hom.), heterozygotes (Het.), and wildtype (WT) siblings used in this paper were F5-F7 generation of repeated backcrosses of nNOS^{S1412A} to C57Bl/6.

Our nNOS^{S1412A} knock-in mutant is available upon request. Please address all inquiries to the corresponding author.

nNOS^{S1412A} eNOS KO: We generated mice doubly homozygous for eNOS knockout and the nNOS^{S1412A} mutation by mating nNOS^{S1412A} and eNOS KO mice.

Reagents and antibodies

Millipore Sigma (Burlington, MA) provided inhibitors of muscarinic (atropine, A0132) and α- (phentolamine, P7547) and β- (propranolol, P0884 adrenergic signaling, inhibitors of cyclooxygenase (indomethacin, I7378) and nNOS/iNOS/eNOS (L-NAME, N5751), the NK-1 agonist substance P (SP; S6883), recombinant PKA (14-440), DTT (D0632), protease inhibitors (PI, P8340), phosphatase inhibitors (PhosI, P5726), 2`,5`-ADP sepharose 4B (GE17-0700-01), and all bulk reagents. ThermoFisher (Waltham, MA) produced myristoylated PKA inhibitor peptide residues 14-22 (Myr-PKI, 77409) and all LC-MS solvents. Cayman Chemical (Ann Arbor, MI) made the inhibitors of PKA (H-89, 10010556) and nNOS/iNOS (1400W, 81520). The Akt inhibitors MK-2206 (MK, A3010) and Akti-1/2 (Akti, ab142088) were from Apex Bio (Houston, TX) and Abcam (Cambridge, Cambridgeshire, UK), respectively. Santa Cruz Biotech (Dallas, TX) produced the PKG inhibitor Rp-8-Br-cGMPs (sc-200323).

ImmunoStar (Hudson, WI) provided rabbit polyclonal anti-nNOS N-terminal peptide residues 134-148 (24431). Abcam produced rabbit polyclonal anti-nNOS peptide residues 1411-1425 phosphorylated at S1412 (ab5583). Cell Signaling (Danvers, MA) generated rabbit monoclonal anti-PKG1 (3248S) and rabbit polyclonal anti-PDE5 (2395S). Cayman Chemical provided rabbit polyclonal anti-sGCβ (160897).

Novus Biologicals (Littleton, CO) produced chicken polyclonal anti-PGP9.5 (NB110-58872). Li-Cor Biosciences (Lincoln, NE) provided goat anti-rabbit IRDye-680RD (925-68071) and goat anti-mouse IRDye-800CW (925-32210). Abcam produced goat anti-chicken Alexa Fluor 488 (ab150169) and goat anti-rabbit Alexa Fluor 594 (ab150080).

Buffers

Krebs: 118mM NaCl + 4.7mM KCl + 1.2mM $MgSO_4 \bullet 7H_2O$ + 25mM $NaHCO_3$ + 1.2mM KH_2PO_4 + 11mM glucose + 5mM HEPES + 50μM EDTA + 3.3mM $CaCl_2$.

Ca^{2+}-free Krebs: $CaCl_2$ was omitted and 100μM EGTA was included.

PBS: 138mM NaCl + 2.7mM KCl + 10mM KH_2PO_4/K_2HPO_4, pH 7.4 at 25 °C.

PBT-2,4: PBS + 0.1, 0.2, or 0.4 % (v/v) Triton X-100.

PBTW: PBS + 0.1% (v/v) Tween-20.

Protein extraction buffer: 25mM Tris-HCl (pH 7.5 at 25 °C) + 1mM EGTA + 1mM DTT + 0.4% (v/v) Triton X-100 + 1x PI + 1x PhosI.

Affinity purification buffer: 100mM Tris-HCl (pH 7.5 at 25 °C) + 150mM KCl + 2mM EGTA+ 2mM EDTA+ 0.4% (v/v) Triton X-100 + 3.3% (v/v) glycerol + 1mM DTT + 50mM NaF + 5mM Na-pyrophosphate + 30mM β-glycerophosphate + 1mM Na-orthovanadate + 2x PhosI + 2x PI.

Affinity wash buffer: 100mM Tris-HCl + 2mM EGTA+ 2mM EDTA + 1mM DTT + 17mM NaF + 1.7mM Na-pyrophosphate + 10mM β-glycerophosphate + 0.3mM Na-orthovanadate + 1x PhosI + 1x PI.

Supplementary Methods

Tissue collection, protein extraction, and immunoblotting

To assess how EFS affects nNOS phosphorylation, we flash-froze ileal rings with liquid nitrogen-chilled forceps immediately following EFS. The lag time between the end of EFS and forceps-mediated tissue vitrification was ≤5 sec. To assess how genotype affects protein expression in **Fig. 4C-D**, we flash-froze

ileal rings from freshly-euthanized animals after brief exposure to Ca^{2+}-free Krebs during ileal lumen perfusion. We extracted ileal protein with ice-cold protein extraction buffer in an equal volume of 0.9-2.0mm diameter stainless steel beads (Next Advance; Troy, NY) subjected to 3 x 5 min pulverization cycles in a Bullet Blender bead mill (Next Advance) at 80% power. We centrifuged homogenates for 10 min at 16,000 x g and retained the supernatant for immunoblotting. We determined protein concentration by the Pierce 660nm protein assay (ThermoFisher). See **SI Appendix Fig. S10** for confirmation of NO signaling pathway antibodies using positive (high expressing) and negative (low expressing) tissues. Purification of phosphorylated ileal nNOS was conducted as before (5) with the following modifications: We extracted protein with affinity purification buffer and incubated 16,000 x g supernatants of 4-8 ileal ring lysates in batch with equilibrated 2`, 5` ADP sepharose 4B at a 2:1 ratio of extract to beads for 3-4 hours at 4 ºC. Beads were washed once with affinity purification buffer, once with affinity wash buffer, and finally eluted at 95 ºC with a 1:1 (v/v) mixture of affinity wash buffer and 6x Laemmli sample buffer.

To visualize protein from tissue lysates, we transferred SDS-PAGE resolved proteins to Immobilon-FL PVDF membranes (ThermoFisher). We washed membranes 3 x 5 min with PBS and blocked for 60 min with 10% (w/v) non-fat dry milk in Licor Odyssey buffer (phospho-nNOS blots) or 2.5% non-fat dry milk in PBS (all other antigens). After blocking, membranes were incubated with primary antibodies overnight at 4 ºC at the following concentrations in PBTW + 2.5% non-fat dry milk: nNOS, 1:500; pS1412 phospho-nNOS, 1:250; PKG1, 1:1000; PDE5, 1:1000; sGCβ, 1:1000. Subsequently, we washed membranes 5 x 5 min with PBTW, blocked with PBTW + 2.5% non-fat dry milk for 15 min, and incubated with IRDye secondary antibodies (Li-Cor) at 1:7500 in PBTW + 2.5% non-fat dry milk for 50 min. We washed membranes 5 x 5 min with PBTW and 2 x 5 min with PBS, after which we visualized proteins with an Odyssey flatbed scanner (Li-Cor). We quantified fluorescence with Li-Cor Image Studio 5.2 and normalized band intensity to appropriate loading controls (total nNOS protein or Ponceau total protein). Housekeeping proteins (e.g., β-actin and GAPDH) are common loading controls, but recent studies suggest that total protein stains (e.g., Ponceau S and Biorad Stain-Free) exhibit less variability and

a larger dynamic range for normalization (6, 7). In our experiments, use of GAPDH as a loading control did not yield significantly different results from Ponceau S.

Organ bath pharmacology

For organ bath experiments, we used 8-26 week old virgin male mice fed a standard chow diet and housed communally or in isolation. We asphyxiated mice by CO_2 and placed the ileum (the lower 40% of the small bowel between the pylorus and ileocecal valve (8)) in ice-cold 95% O_2/5% CO_2 (95/5)-treated Ca^{2+}-free Krebs buffer. Ca^{2+}-free solutions enhance ex vivo contractility of smooth muscle preparations following reintroduction of Ca^{2+} (9). We removed the mesentery with scissors, discarded the 10mm of ileum closest to the ileocecal valve, and flushed the ileum of solid contents with Ca^{2+}-free Krebs using an 18-gauge blunt tip syringe. We then cut the cleaned ileal segment into 5-10mm long tissue rings and applied fresh Ca^{2+}-free Krebs.

We performed organ bath experiments at 37 ^{o}C in two 159920-X1/10 systems (Radnoti; Covina, CA) containing eight 10ml glass chambers and two solvent reservoirs for 95/5-perfused Krebs buffer. Both systems were housed in a glass-encased water jacket maintained at 37 ^{o}C and circulated by a 170051B water heater-pump (ThermoFisher). We monitored ileal tension with MLT0201/RAD force transducers (AD Instruments; Colorado Springs, CO), which were positioned above chambers and coupled to Powerlab 16/35 (AD Instruments) with LabChart7.0 output (AD Instruments). Before mounting ilea, we placed platinum electrodes (Radnoti 160152-14) in all chambers. An S88 Grass stimulator (Natus; West Warwick, RI) nominally supplied 40V to each electrode via a 4-port diverter (Radnoti 159981).

To mount ileal segments, we inserted silk-threaded 10mm triangular pins (Radnoti 158817) into ileal segment lumens, suspended silk strings from force transducers, placed pin-threaded ilea in Krebs-filled chambers, and inserted electrode support pins into ileal segments to generate tensile force. We added atropine (1μM), propranolol (1μM), phentolamine (1μM), and indomethacin (10μM) to chambers

containing ileal rings that exhibited spontaneous contractile activity within 15 minutes of mounting, thus affording non-adrenergic, non-cholinergic (NANC) conditions (10, 11). 10 minutes after onset of NANC conditions, we added substance P (1μM) to stimulate regular contractions (12). After cessation of tetanus and with a stable baseline, we applied cumulative electric field stimulation (EFS) for 300 seconds with 2msec pulse width square waves of 20 V and 30 sec train duration at 0.25Hz, 0.5Hz, 1.0Hz, 2.0Hz, 4.0Hz, and 8.0Hz. After the final 8.0Hz stimulation, we turned the stimulator off and recorded an additional 30 seconds of contractility. We did not analyze ileal segments that did not contract with substance P or that did not demonstrate post-EFS contractility.

We used LabChart 7 to quantify the mean tensile force for each ileal segment. Mean tensile force is the definite integral (area under the curve, or AUC) of the force function divided by the time interval. We normalized mean tensile force at each EFS frequency to F_{SP}, defined as the mean baseline tension with substance P (t_{max}) after tetany and before the first EFS train ($t_{0.25}$). We calculated F_{SP} as follows:

$$F_{SP} = (AUC_{total} - AUC_{0.25\text{-}end})/(t_{0.25}-t_{max})$$

Where the AUC_{total} is AUC from t_{max} to 30 seconds after stimulation (t_{end}), calculated with respect to the minimum value of the force function. (see **SI Appendix Fig. S11**).

Mean tensile forces at each EFS frequency were derived similarly:

$F_{0.25}$ (mean force at 0.25Hz EFS) = $(AUC_{0.25\text{-}end} - AUC_{0.5\text{-}end})/(t_{0.5}-t_{0.25})$;

$$F_{0.5} = (AUC_{0.5\text{-}end} - AUC_{1.0\text{-}end})/(t_{1.0}-t_{0.5})$$
$$F_{1.0} = (AUC_{1.0\text{-}end} - AUC_{2.0\text{-}end})/(t_{2.0}-t_{1.0})$$
$$F_{2.0} = (AUC_{2.0\text{-}end} - AUC_{4.0\text{-}end})/(t_{4.0}-t_{2.0})$$
$$F_{4.0} = (AUC_{4.0\text{-}end} - AUC_{8.0\text{-}end})/(t_{8.0}-t_{4.0})$$
$$F_{8.0} = (AUC_{8.0\text{-}end} - AUC_{off\text{-}end})/(t_{off}-t_{8.0})$$
$$F_{off} = AUC_{off\text{-}end}/(t_{end}-t_{off})$$

Where t_{off} is the time that stimulation ended. If an ileal segment's force function minimum did not coincide with t_{off}, then the time at which the minimum tension did occur (t_{min}) was the upper limit of integration prior to t_{min} and the lower limit of integration after t_{min}.

To measure sodium nitroprusside (SNP)-induced relaxation, we added cumulatively increasing concentrations of SNP every 2 min. As before, we normalized mean tensile force at each SNP concentration to the tensile force 5 min after adding substance P. To measure effects of MK-2206 (10μM), Akti-1/2 (10μM), H-89 (10μM), Myr-PKI (30μM), L-NAME (1mM), and TTX (10μM), we added these compounds under NANC conditions before adding substance P, using previously published concentrations sufficient to inhibit targets but low enough to avoid tissue damage and apoptosis (13-18). The vehicle was 0.1% (v/v) DMSO or water as appropriate. **SI Appendix Fig. S12** contains representative force-time tracings from organ bath experiments.

nNOS purification, kinase assay, and mass spectrometry for nNOS^{S1412A} mutation

We purified nNOS from nNOS^{S1412A} WT, Het., and Hom. sibling brains with 2`,5`-ADP sepharose 4B and assayed nNOS S1412 phosphorylation with PKA as before (5). To confirm expression of nNOS^{S1412A}, we prepared partially-purified brain nNOS samples for mass spectrometry sequencing using LC-MS grade solvents. We resolved samples by SDS-PAGE, stained gels with colloidal Coomassie blue, destained gel pieces containing bands 125-160kDa in 200 μL 25 mM ammonium bicarbonate in 50 % (v/v) acetonitrile for 15 min, washed with 200 μL 50% (v/v) acetonitrile, treated with 10 mM DTT at 60 °C for 30 min, and alkylated with 20 mM iodoacetamide (IAA) in the dark at room temperature for 45 min. We sequentially washed gel pieces with 100 μL water and 100 μL acetonitrile, dried via speed vac, rehydrated at 4 °C in the presence of 100 ng trypsin (Millipore Sigma) for 45 min, and incubated at 37 °C overnight. Tryptic mixtures were brought to 1% (v/v) formic acid + 50% acetonitrile (v/v), and peptide enriched supernatants were dried via speed vac.

For LC peptide fractionation, we used an easy nanoLC 1000 liquid chromatograph (ThermoFisher) and a 2.7 μm Phenomenex Cortecs C18 resin analytical column (100 μm x 10 cm) equilibrated in 0.1% formic acid. Upon sample loading, we employed a 70-min, 4-32% acetonitrile linear gradient run at 400nL/min. Column eluate flowed through a nanospray ionization source of a Q Exactive quadrupole orbitrap mass

spectrometer (ThermoFisher). The Q Exactive was operated in positive ion mode with a target value of $1*10^6$ ions/50msec maximum injection time, and data was acquired with Xcalibur™ 3.0 (ThermoFisher). Parent peptide ions were detected at resolution 70,000 (FWHM at m/z 200) in orbitrap mode. For tandem mass spectrometry, the Q Exactive subjected the 15 most abundant ions (1.2 m/z isolation window) to HCD fragmentation and detected at resolution 17,500 (AGC target: $1*10^5$). We used Scaffold 4.3.2 (Proteome Software; Portland, OR) to resolve mass chromatograms (19). Parent and fragment ion mass tolerance were 2 Da and 0.1 Da, respectively, the peptide identification probability threshold (via Peptide Prophet) was 95%, and one missed cleavage by trypsin was allowed. We analyzed two or more biological replicates for WT and $nNOS^{S1412A}$ samples. Total nNOS sequence coverage varied from 56-67%.

Organ histology and immunofluorescence

For histology, we fixed organs from freshly euthanized animals in Bouin's solution overnight. Paraffin-embedded organs were sectioned with a microtome, mounted onto glass slides, and deparaffinized. A subset of slides were used for immunofluorescence while others were stained with Masson's trichrome or H&E. To quantify ileal and colonic submucosal and myenteric ganglia at 400x magnification, we examined 9-12 H&E and trichrome-stained samples from 2 or more mice using a BH-2 microscope (Olympus Life Science; Waltham, MA). All quantification was performed on 400x magnified images, but the representative colonic micrographs in SI Appendix Fig. S5 were recorded at 200x. We obtained whole mounts of ileum myenteric plexus (MP) and adjoining longitudinal smooth muscle (LM) as described previously (20, 21). Briefly, we inserted a glass rod into the lumen of 5cm of terminal ileum excised after euthanasia and extracted the MP and LM by rubbing forceps over the gut tube until a gap formed in the LM, which permitted removing the muscle layer with a PBS-soaked cotton swab. The resulting tissue was fixed in 4% (w/v) paraformaldehyde and stored in PBS at 4 ^oC for up to 3 months.

For immunofluorescence, we microwaved deparaffinized slides 5 min in a citrate-based buffer (Abcam). After antigen retrieval, we processed slides and whole mounts identically using 0.22μm membrane-

filtered solutions. After washing slides or whole mounts in PBS, we permeabilized samples with 300mM glycine + PBS for 30 min, rinsed with PBS 3 x 5 min, blocked with 5% (w/v) goat serum + 5% (w/v) horse serum + 1% (w/v) BSA in PBT-4 for 60 min, and incubated with antibodies against nNOS (1:500) and the pan-neuronal marker PGP9.5 (1:500) in PBT-2 + 1% BSA at 4 ^{o}C overnight. We then washed samples with PBT-2, blocked with 2.5% goat serum + 2.5% horse serum + 1% BSA in PBT-2 for 10 min, and incubated in the dark for 60 min at room temperature with Alexa Fluor 488 and 594-conjugated goat antibodies against chicken and rabbit, respectively (1:1000 each in PBT-2 + 1% BSA). We rinsed samples with PBT-2 4 x 5 min, followed by PBS 2 x 5 min. We visualized slides and whole mounts with an Olympus CKX41 widefield fluorescence microscope and an Olympus FV1000 laser scanning confocal fluorescence microscope, respectively.

Gastrointestinal Motility Monitor (GIMM) setup and data analysis

The gastrointestinal motility monitor (GIMM; Catamount Research and Development; St. Albans, VT) (22-24) is a 37 ^{o}C-jacketed chamber filled with circulating 95/5-perfused Krebs buffer that enables ex vivo measurement of intestinal motility. GI segments are extended to limit elastic lateral displacement to ≤1cm and immobilized with pins to a foam pad at the bottom of the chamber. A camera with a line of sight perpendicular to the chamber records a top-down video of the GI segment's propagating and mixing contraction patterns. Users define a region of interest to encompass the GI segment, and the GIMM software applies a binary intensity mask to digitally distinguish the GI segment (black) from surrounding buffer (white). To construct 2-dimensional spatiotemporal (ST) map jpeg files for analysis in ImageJ (described below), the intensity at each pixel length is averaged across all widths for every pixel unit time. For a 5cm GI segment, ST maps are 112 pixels/cm (length) x 18 pixels/sec (time). Forward time is oriented downward, and the GI segment oral end faces to the left. ST maps may reveal both propagation and mixing by a GI segment. *Propagation* (peristalsis) refers to unidirectional propulsion generated by relaxation on one side (typically anal) and contraction on the other side (typically oral). Anterograde propagating waves appear as parallel lines extending diagonally and down to the right (negative slope),

while retrograde propagating waves extend up to the right. *Mixing* (or segmentation) refers to bidirectional, non-propulsive movement caused by similar muscle tone on both sides of a wave that cyclically alternates between contraction and relaxation. Mixing waves appear as irregular sinusoids (25, 26). Mixing distance is sinusoidal arc length and corresponds to how fast and over how much GI segment length a mixing wave occurs.

Following mouse euthanasia, we trimmed mesentery from 5cm terminal ileum segments (measured from the ileocecal junction) in ice-cold Krebs buffer and placed ilea into the GIMM. We did not use NANC inhibitory compounds. We traced propagation waves in ST map .jpegs to determine propagation speed (defined as the slope of each line) using the GIMM ImageJ plug-in (27). We determined percentages of segments that propagate by measuring the x-axis distance from beginning to end of a propagation and dividing by the GI segment length (we excluded propagations that crossed the top or bottom x-axis). Propagation frequency was equal to the number of propagations per unit time. We determined mixing distance with ImageJ by setting the aspect ratio to zero and measuring the distance of 3-7 mixing waves by freehand tracing. Mixing frequency was equal to the average number of wave crests in 3-7 mixing waves per unit time. See **Fig. 5A** and **SI Appendix Fig. S13** for illustrations of GIMM setup and data analysis.

Statistical tests

We performed all statistical tests with the GraphPad Prism 7.04 software (La Jolla, CA) and chose a significance threshold of $p<0.05$. For comparisons among three or more conditions, we employed one-way analysis of variance (ANOVA). We conducted Dunnett or Tukey post-tests when ANOVA yielded significant results. We used Dunnett tests for comparisons of experimental conditions to a control or vehicle condition, and we used Tukey tests to compare all conditions or genotypes to one another. For Dunnett tests, asterisks (*) refer to treatments that are significantly different from the vehicle control. For

Tukey tests, different letters (e.g., *a, b, c*) refer to groups that are significantly different from each other (i.e., *a* is significantly different from both *b* and *c*, whereas *ab* is indistinguishable from both *a* and *b*). For tensile force measurements, we performed ANOVA and post-tests at each EFS frequency. We derived IC_{50} values by non-linear logistic regression using a log [agonist] model with null hypothesis: one curve explains data. For mice used in GIMM studies, we applied analysis of covariance (ANCOVA) to simple linear regression models correlating weight, age, propagation speed, and mixing distance (null hypotheses: identical regression line slopes and intercepts). We conducted all experiments with 3 or more ileal rings obtained from 2 or more mice.

Supplementary Figures

SI Appendix Fig. S1

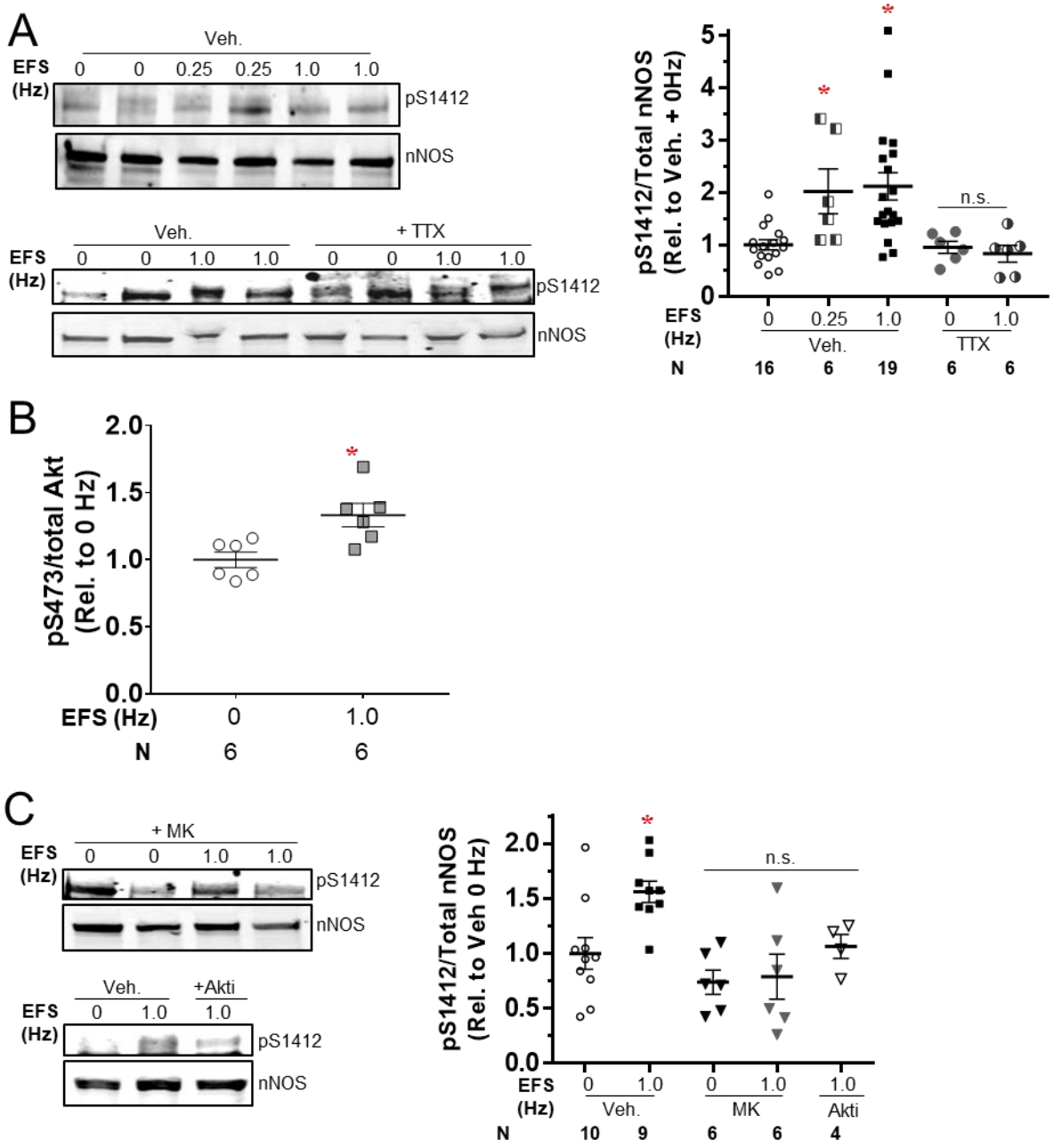

Quantification of neuronal depolarization-stimulated phosphorylation of nNOS S1412 and Akt S473 in crude lysates. A. Low and medium frequency EFS induces nNOS S1412 phosphorylation, but TTX prevents EFS-induced nNOS S1412 phosphorylation. *Left*: Representative immunoblots. *Right*:

Quantification of pS1412/total nNOS ratio relative to unstimulated vehicle controls. Veh: vehicle, 0.1% (v/v) DMSO. Error bars: SEM. *: $p<0.05$ vs. Veh + 0 Hz by Dunnett test. n.s.: not significant. N: number of ileal rings. B. Quantification of pS473/total Akt ratio relative to unstimulated controls. N: 4-8 pooled ileal rings for each lysate. C. Akt inhibitors curtail EFS-induced nNOS S1412 phosphorylation. N: number of ileal rings.

SI Appendix Fig. S2

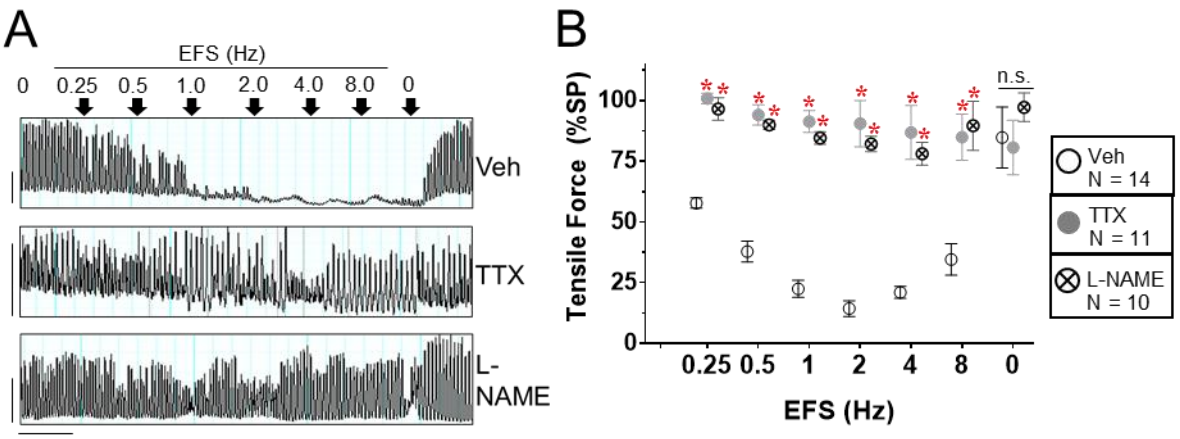

EFS-induced ileal relaxation requires neuronal depolarization and NOS activity. A. Inhibition of NOS activity (L-NAME; 1mM) or neuronal depolarization (TTX; 10μM) prevents EFS-induced ileal relaxation. Veh: vehicle, 0.1% (v/v) DMSO. Scale bars: 0.07g (vertical), 30sec (horizontal). B. Quantification of A. Error bars: SEM. *: $p<0.05$ vs. Veh at each frequency by Dunnett test. N: number of ileal rings.

SI Appendix Fig. S3

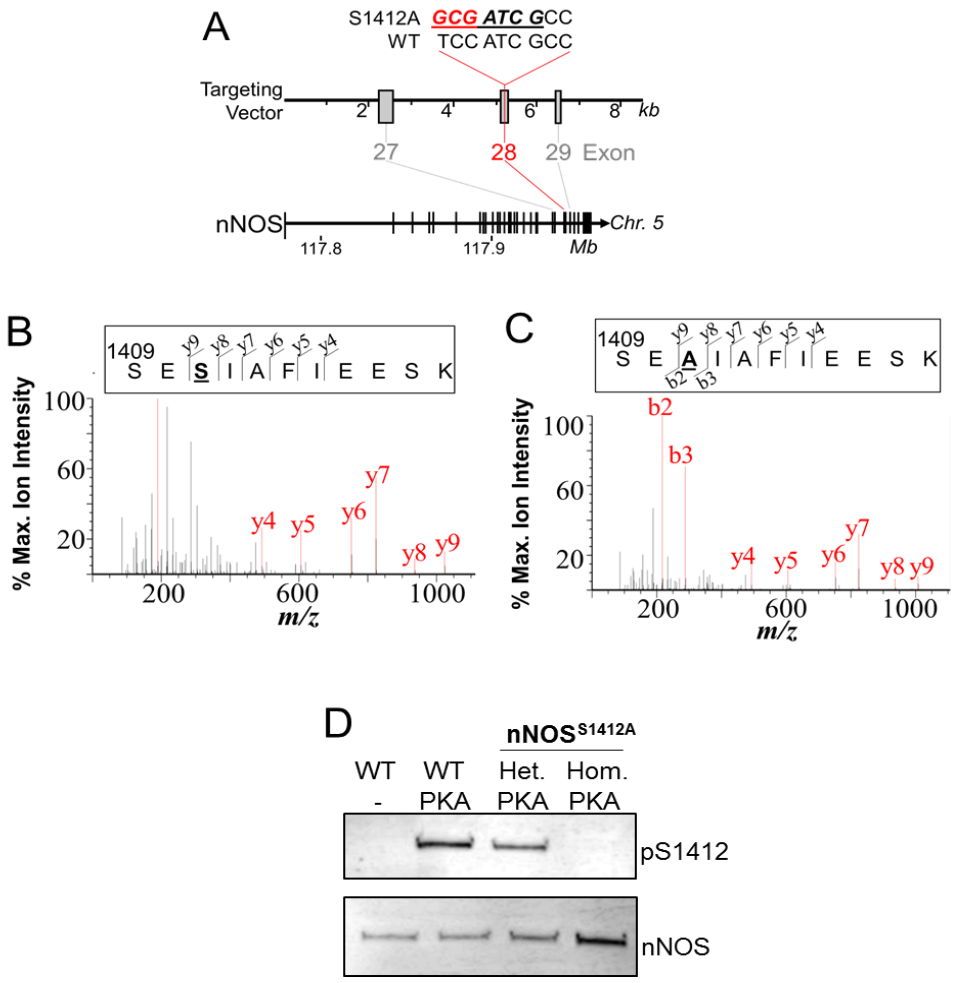

Validation of the nNOS^{S1412A} mutation. A. Cloning strategy to produce the nNOS^{S1412A} knock-in mutant mouse. The targeting construct is homologous to nNOS exon 28 and replaces the Ser1412 codon with an Ala codon. B-C. Mass spectrometry of nNOS partially purified from brains of WT (B) and nNOS^{S1412A} Hom. siblings (C) confirms expression of the mutant nNOS^{S1412A} protein. MS2 spectra are shown for the tryptic peptide containing amino acid 1412 of nNOS (highlighted in bold). b and y ions (+1 charge state) are shown in red. D. The nNOS^{S1412A} mutation blocks in vitro PKA-dependent phosphorylation of brain nNOS between residues 1411 and 1425.

SI Appendix Fig. S4

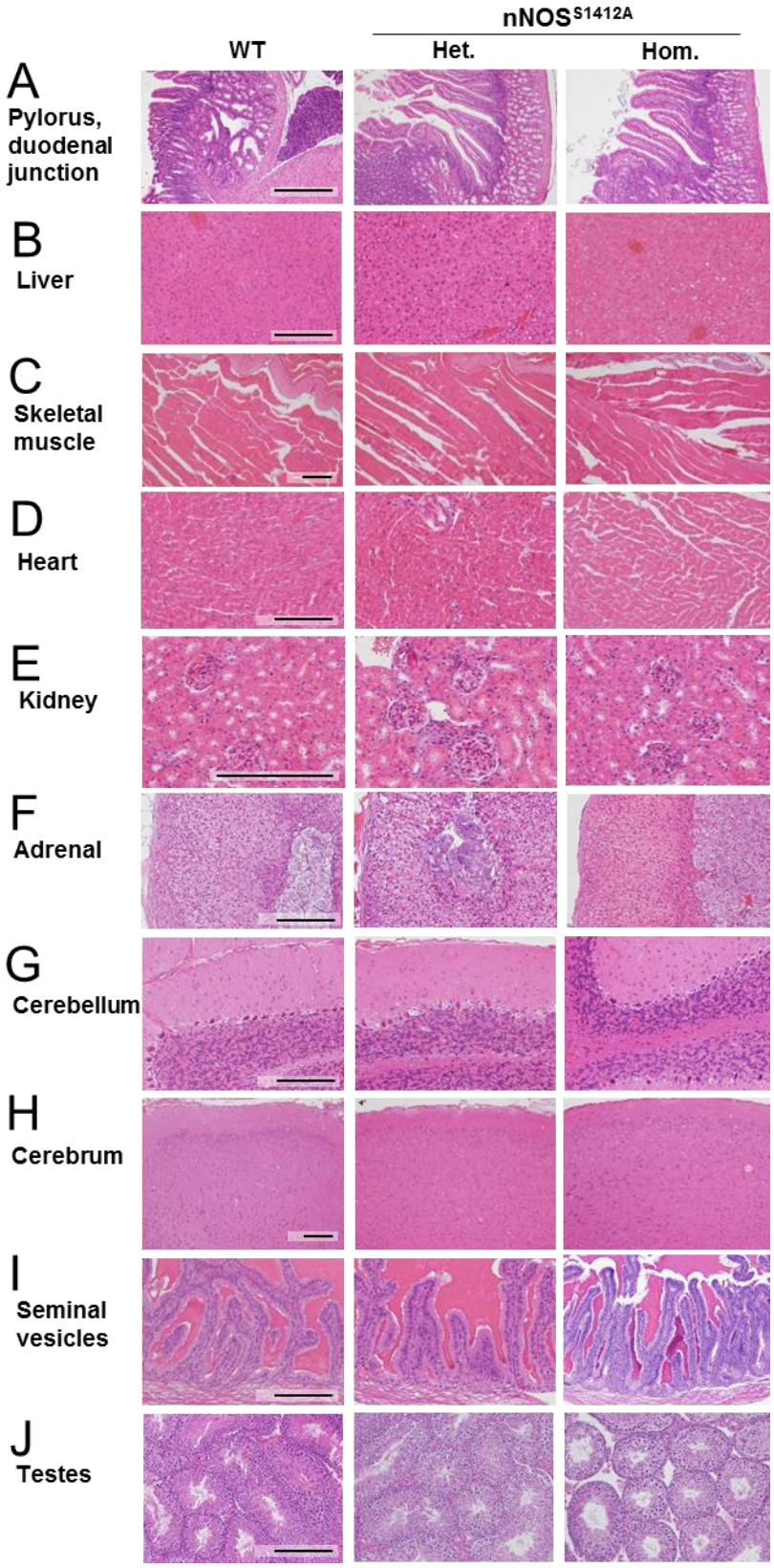

nNOS^{S1412A} mice exhibit normal internal organ histology. Representative formalin fixed paraffin embedded (FFPE) sections stained with hematoxylin and eosin. A. Pylorus and duodenal junction. B. Liver. C. Skeletal muscle. D. Heart. E. Kidney. F. Adrenal. G. Cerebellum. H. Cerebrum. I. Seminal vesicle. J. Testis. Scale bar: 200μm.

SI Appendix Fig. S5

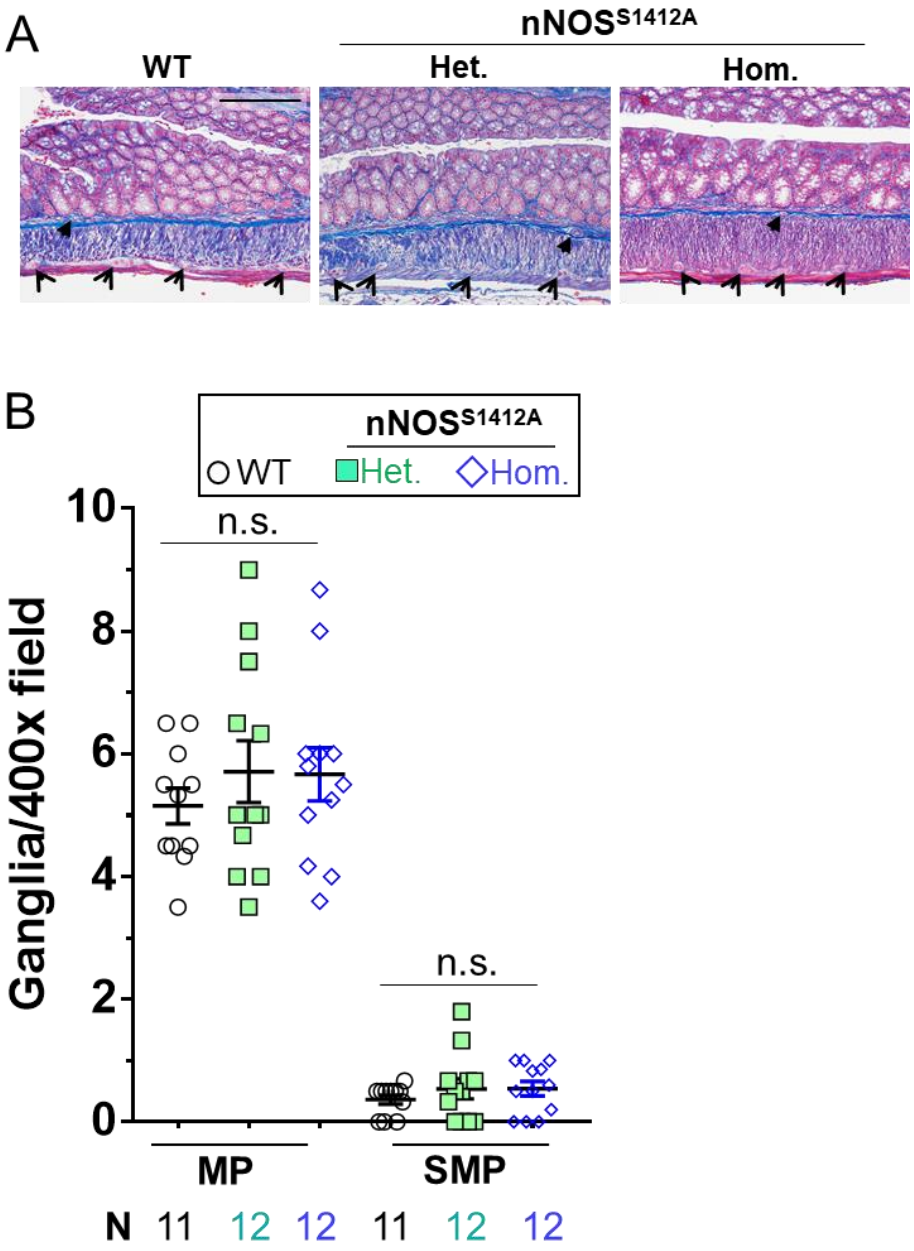

nNOS^{S1412A} mutants exhibit normal colonic histology. A. Representative FFPE sections of colon stained with Masson's trichrome. Black arrowheads denote ganglia. Scale bar: 200µm. B. nNOS^{S1412A} mutants have normal numbers of colonic myenteric and submucosal ganglia. Error bars: SEM. MP: myenteric plexus. SMP: submucosal plexus. n.s.: not significant by one-way ANOVA. N: number of 400x micrographs analyzed.

SI Appendix Fig. S6

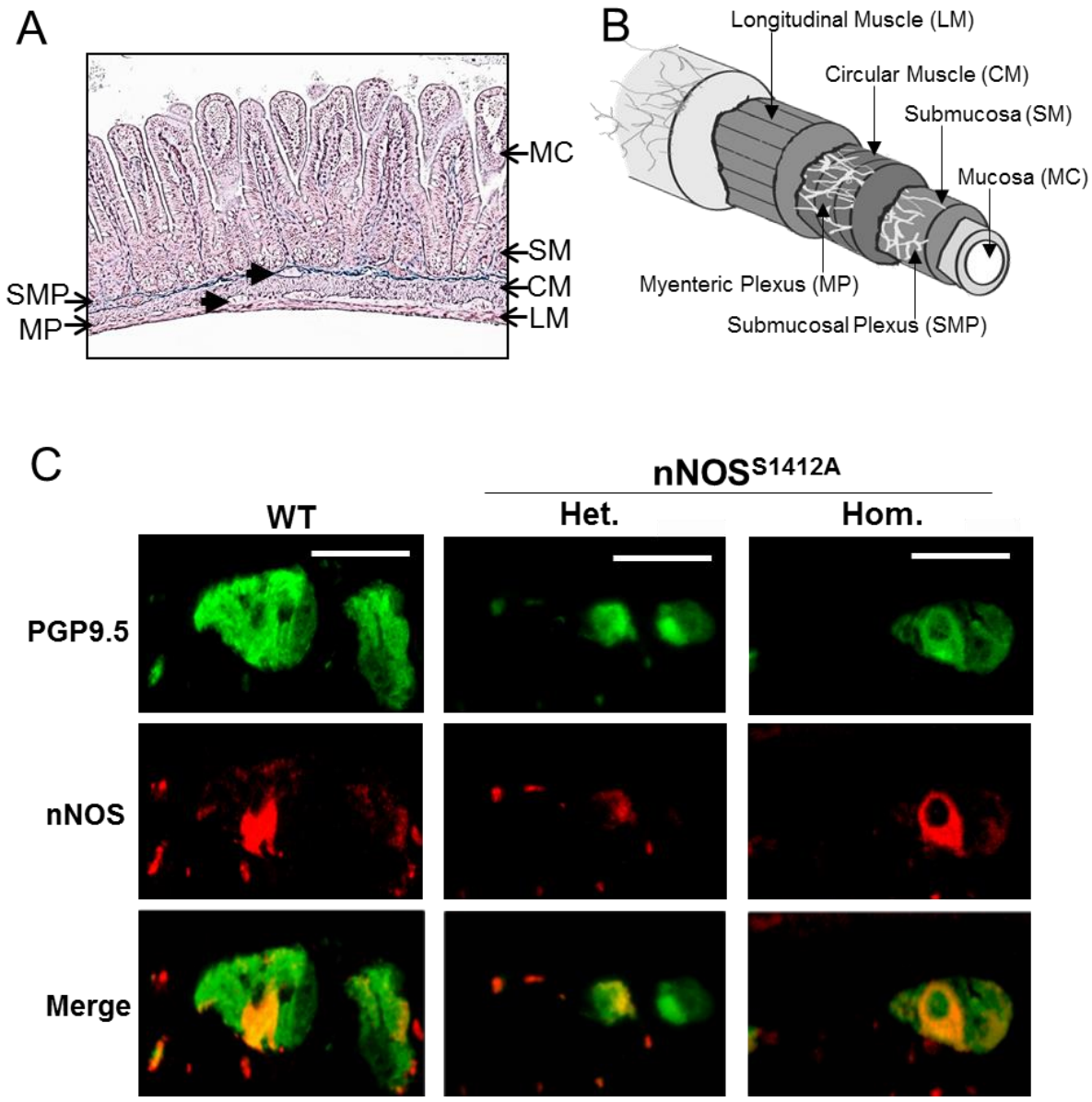

The nNOS^{S1412A} mutation does not alter the distribution of nNOS within myenteric ganglia. A-B. Longitudinal (A) and transverse (B) cross-section illustrations of ileum. MC: mucosa. SM: submucosa. SMP: submucosal plexus. CM: circular smooth muscle. MP: myenteric plexus. LM: longitudinal smooth muscle. Arrowheads: SMP and MP ganglia. C. Longitudinal FFPE sections of ileum from WT and nNOS^{S1412A} Het. and Hom. mice stained with antibodies against nNOS (red) and PGP9.5 (green). PGP9.5 and nNOS localize to MP ganglia. Scale bar: 50µm.

SI Appendix Fig. S7

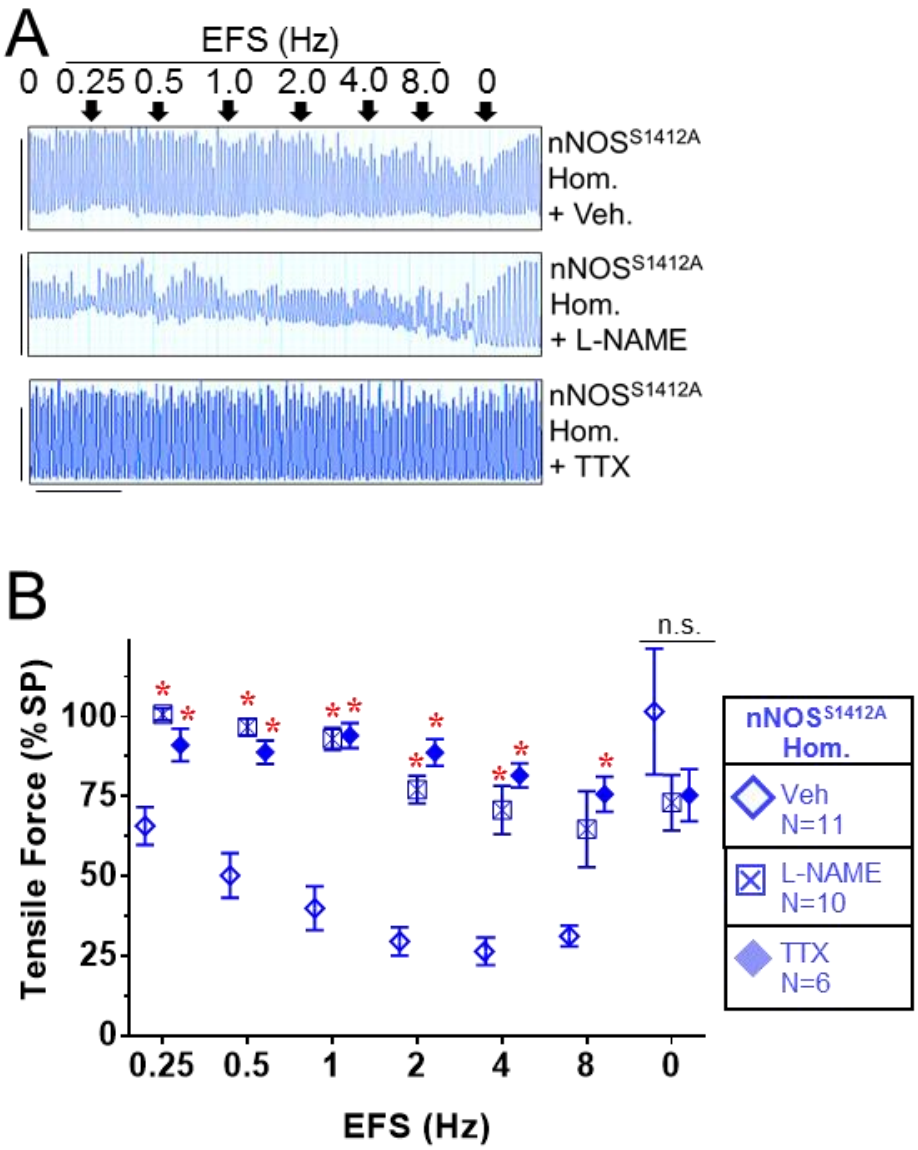

EFS relaxation of ileal rings from nNOS^{S1412A} homozygotes requires NOS activity and neuronal depolarization. A. EFS-induced relaxation of nNOS^{S1412A} Hom. ileal rings is sensitive to the pan-NOS inhibitor L-NAME (1mM) and the neuronal depolarization inhibitor TTX (10µM). Scale bars: 0.11g (vertical), 30sec (horizontal). B. Quantification of A. *: $p<0.05$ vs. Veh by Dunnett test. n.s.: not significant. N: number of ileal rings. Error bars: SEM.

SI Appendix Fig. S8

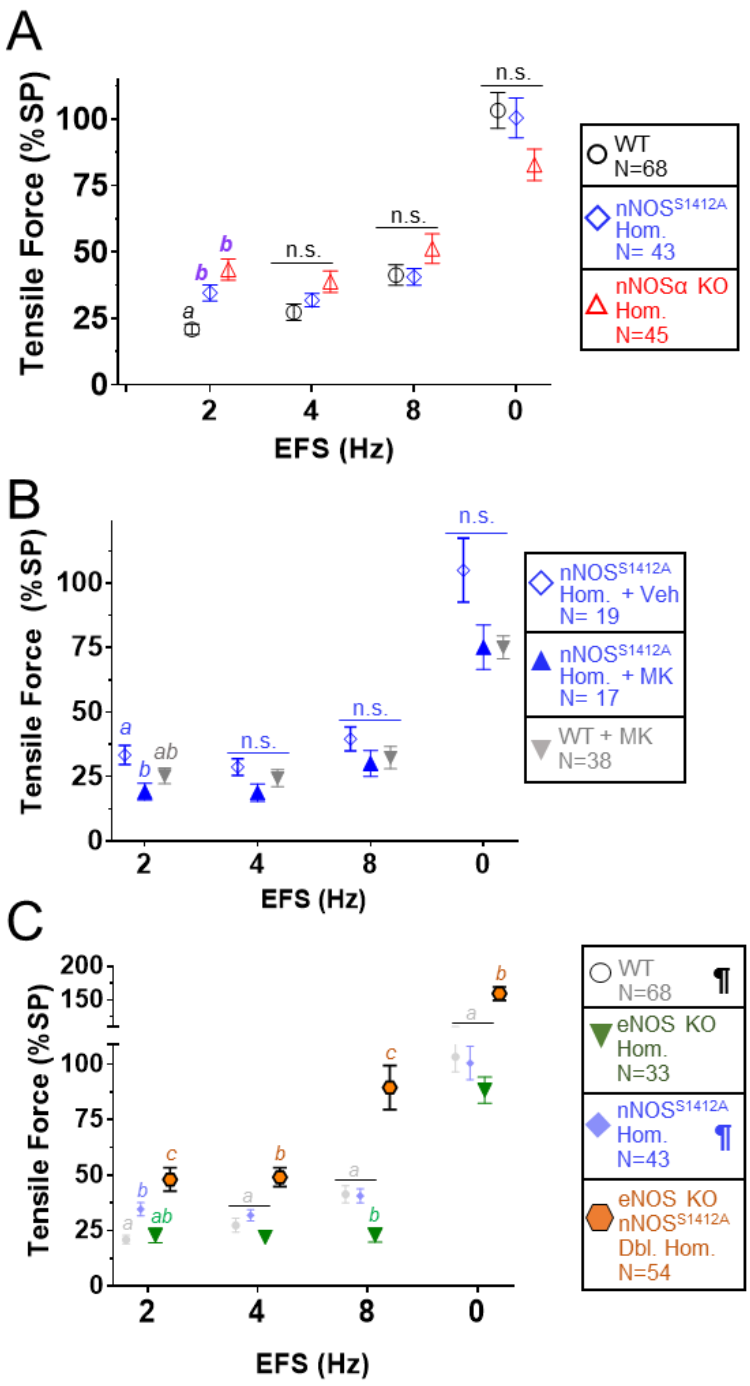

High frequency EFS relaxation of ileal rings. A-C. EFS relaxation at high frequency for WT, nNOS^{S1412A}, and nNOSα KO ilea (A); MK-treated WT and nNOS^{S1412A} ilea (B); and eNOS KO and eNOS KO/nNOS^{S1412A} double mutant ilea (C). ¶: Data repeated from Fig. S8A for comparison. Different letters:

371 $p<0.05$ via Tukey test at each EFS frequency. n.s.: not significant. N: number of ileal rings. Error bars:

372 SEM.

SI Appendix Fig. S9

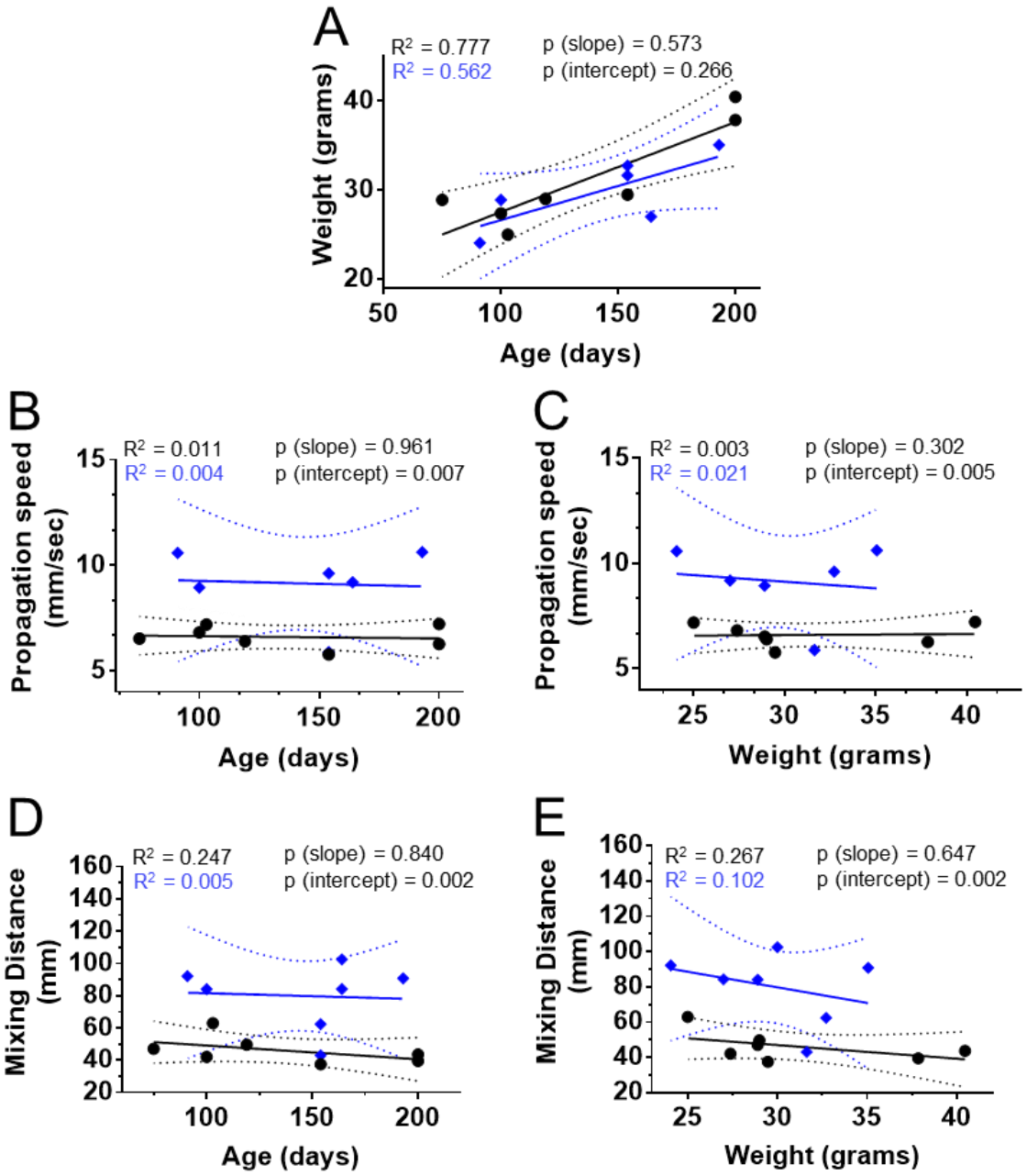

Age and weight do not predict propagation speed or mixing distance in wildtype (●) or nNOS^{S1412A} homozygous (♦) mice. Black and blue regression lines denote WT and nNOS^{S1412A} Hom. mice, respectively. 95% confidence intervals for simple linear regressions are denoted with dotted lines. R^2 values denote squared Pearson correlation coefficients. We employed analysis of covariance (ANCOVA)

379 to test the null hypotheses that WT and nNOS^{S1412A} Hom. mice produce linear regressions with identical
380 slopes and intercepts. A. Age and weight are positively correlated in WT and nNOS^{S1412A} Hom. mice, but
381 the linear relationship between age and weight is not significantly different between WT and nNOS^{S1412A}
382 Hom. B-C. Propagation speed is not correlated with age or weight in WT or nNOS^{S1412A} Hom. mice. D-E.
383 Mixing distance is not correlated with age or weight in WT or nNOS^{S1412A} Hom. mice.

SI Appendix Fig. S10

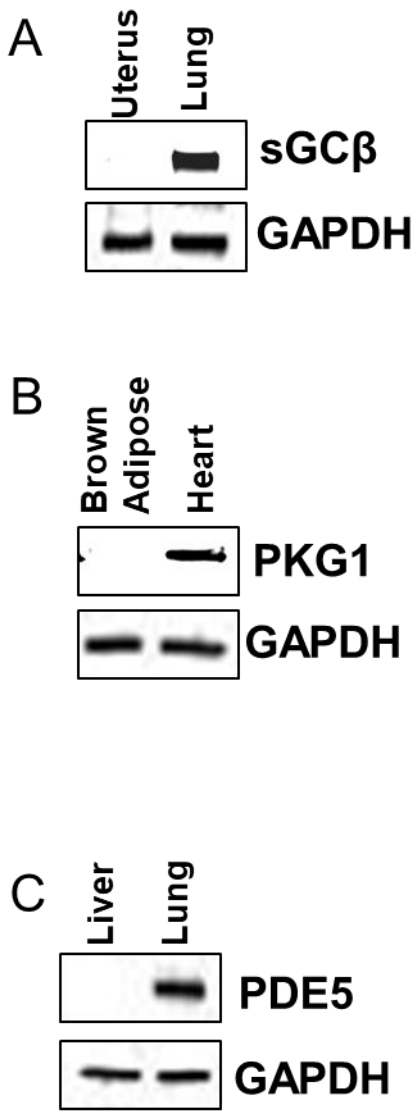

Validation of NO-cGMP pathway antibodies. A-C. Immunoblots with commercial antibodies against soluble guanylate cyclase β (sGCβ), cGMP-dependent protein kinase G-1 (PKG1), and phosphodiesterase-5 (PDE5). GAPDH: loading control. Positive and negative controls were selected from WT tissues that express high and low levels of the indicated target protein. Antibodies recognized a single band of the appropriate molecular weight with expression matching previously published data and gene expression databases.

SI Appendix Fig. S11

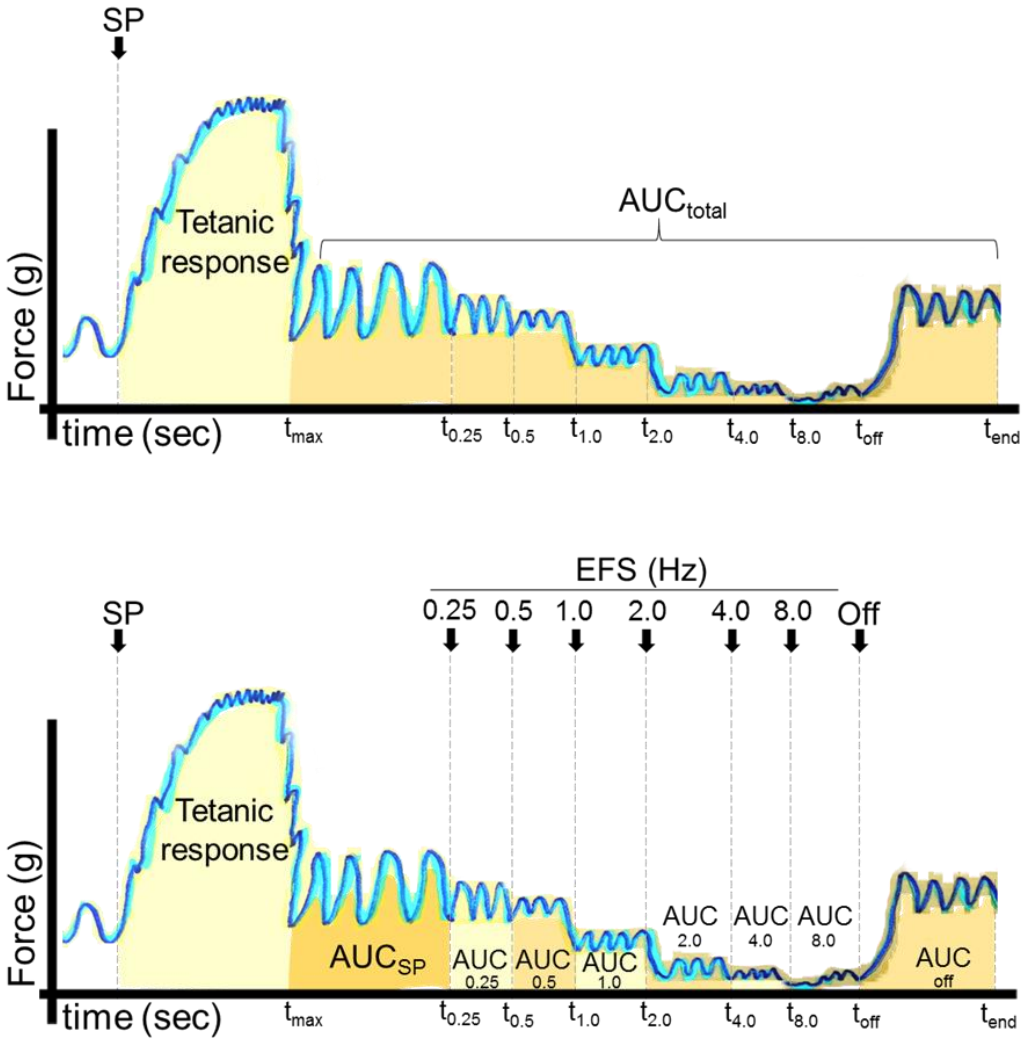

$$F_{SP} = \frac{\int_{t_{max}}^{t_{0.25}} F(t)dt}{(t_{0.25} - t_{max})}$$

Illustration of ileal contraction quantification procedure. The blue trace represents the force tension curve of a spontaneously contracting ileal segment under NANC conditions during substance P (SP)-induced excitation and EFS-induced relaxation. AUC: area under the curve.

SI Appendix Fig. S12

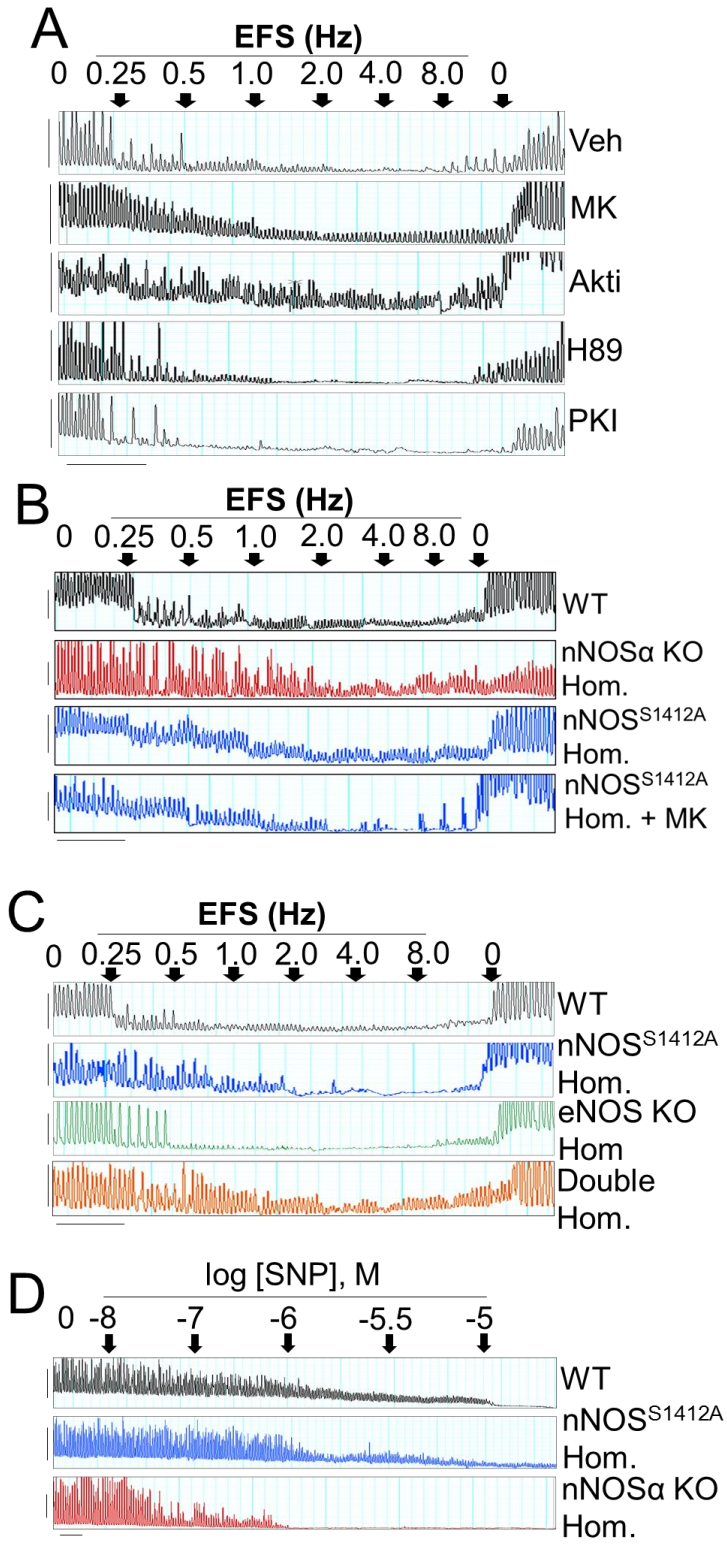

Representative force-time plots for organ bath experiments. A. Representative tracings for Fig. 1C-D. Akt inhibitors (MK, Akti) suppress ileal relaxation at low EFS frequencies, but PKA inhibitors (H89, PKI) do not. Scale bars: 0.1g x 30sec. B. Representative tracings for Fig 3. nNOS^{S1412A} mutant ilea are less sensitive to EFS-induced relaxation than WT, but more sensitive than nNOSα KO. Akt inhibition does not reduce EFS relaxation of nNOS^{S1412A}. Scale bars: 0.05g x 30sec. C. Representative tracings for Fig 4A. eNOS KO ilea are as sensitive to EFS relaxation as WT, and the eNOS KO mutation does not alter low frequency EFS relaxation of nNOS^{S1412A}. Double. Hom: eNOS KO nNOS^{S1412A} double mutant. Scale bars: 0.04g x 30sec. D. Representative tracings for Fig 4B. Compared with WT, nNOS^{S1412A} and nNOSα KO ilea are more sensitive to sodium nitroprusside (SNP)-induced relaxation. Scale bars: 0.04g x 30sec.

SI Appendix Fig. S13

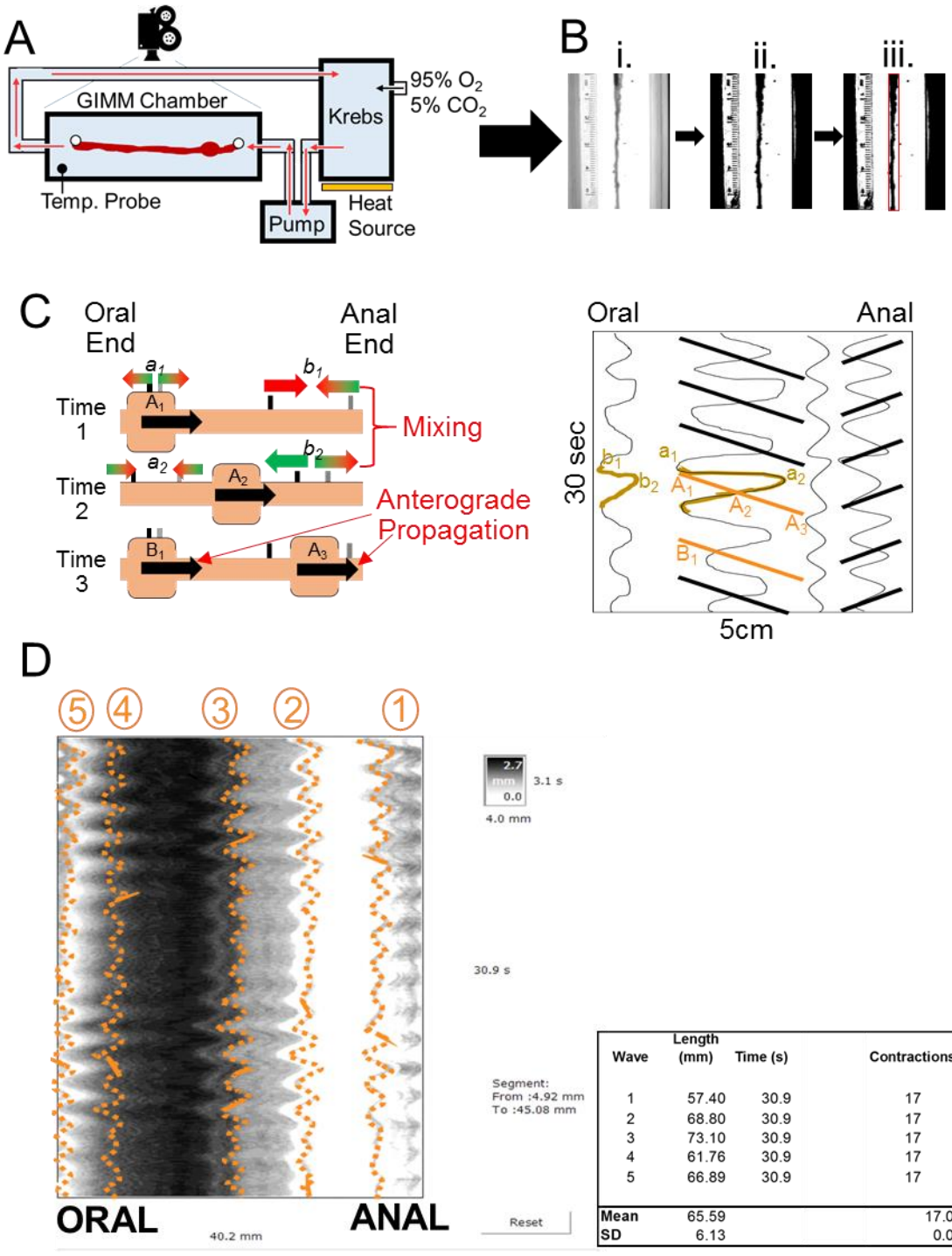

GIMM instrument setup, data collection, and analysis. A. GIMM design. A GI segment (dark red) is immobilized by two pins (white circles) in the GIMM chamber, which is filled with circulating,

oxygenated Krebs solution. A camera is mounted above the GI segment to record motions of the GI segment. B. Data acquisition workflow using the GIMM software. The initial video (i.) is subjected to a binary intensity mask (ii), and a region of interest is drawn (red box) (iii). C. Cartoon depicting the correlation between motions of the GI segment in the region of interest (left) and the resulting ST map (right). Black block arrows (left) denote anterograde propagating waves and are labeled with capital letters with subscript numbers that refer to the time. The two anterograde propagations that occur during the specified time window in the GI segment schematic are highlighted in orange in the ST map schematic. Red and green block arrows denote mixing waves and are labeled with lowercase letters and subscript numbers that correspond to the time. The two mixing waves that occur during the specified time window in the GI segment schematic are highlighted in dark yellow in the ST map schematic. The black and grey rectangles in the GI segment schematic denote small symmetry aberrations such as pieces of mesentery that enable detection of mixing waves. D. Mixing contraction quantification example. 5 evenly-spaced mixing waves in the given ST map are chosen to estimate the average distance traversed by a mixing wave in this ileal segment. The length of each mixing wave corresponds to the mixing distance.

SI Appendix Table S1

Genotype	WT (n=7)	nNOS^{S1412A} Het. (n=7)	nNOS^{S1412A} Hom. (n=7)	ANOVA p
Age (d)	179 ± 30.6	241 ± 35.7	137 ± 25.7	0.082
Whole Body (g)	35.5 ± 2.6	31.8 ± 2.3	30.9 ± 1.0	0.273
Brain (mg)	456 ± 12	419 ± 21	451 ± 6	0.17
Heart (mg)	193 ± 9	179 ± 15	161 ± 7	0.144
Adrenal (mg)	14 ± 1	14 ± 1	13 ± 1	0.891
Kidney (mg)	483 ± 18	507 ± 43	435 ± 32	0.303
Liver (mg)	1693 ± 76	1858 ± 95	1559 ± 90	0.078
Stomach (mg)	357 ± 25	413 ± 43	358 ± 18	0.346
Spleen (mg)	77 ± 4	103 ± 12	96 ± 5	0.077
Testes (mg)	356 ± 24	333 ± 26	306 ± 22	0.361
Sem. Vesicles (mg)	362 ± 33	394 ± 14	318 ± 12	0.075

Organ weights of male nNOS^{S1412A} WT, heterozygous, and homozygous siblings. Mean values and SEMs are shown. Statistical significance was assessed by one-way ANOVA.

SI Appendix Table S2

Parameter	Unit	Mean Value			ANOVA p	Post-test p	
		WT (N = 7)	nNOS^{S1412A} Het. (N = 8-9)	nNOS^{S1412A} Hom. (N = 6-7)		WT *vs* Het	WT *vs* Hom
Propagation speed	mm* s^{-1}	6.6 ± 0.197	7.73 ± 0.420	9.14 ± 0.710	**0.0055**	0.156	**0.003**
Percent of Ileal Segment that Propagates (Total)	%	69.1 ± 7.97	65.7 ± 6.66	67.4 ± 11.7	0.9593	0.941	0.986
Percent of Ileal Segment that Propagates Anterograde.	%	58.5 ± 11.1	35.5 ± 10.2	18.5 ± 8.59	**0.0483**	0.201	**0.03**
Percent of Ileal Segment that Propagates Retrograde.	%	11.0 ± 7.13	29.7 ± 12.1	47.9 ± 16.7	0.1497	0.445	0.098
Propagation Frequency	s^{-1}	0.598 ± 0.030	0.576 ± 0.005	0.554 ± 0.008	0.2771	0.579	0.197
Mixing Distance	mm	46.1 ± 3.23	53.9 ± 3.36	79.9 ± 7.69	**0.0004**	0.433	**0.0003**
Mixing Frequency	s^{-1}	0.645 ± 0.032	0.581 ± 0.005	0.575 ± 0.010	**0.0394**	0.051	**0.047**
Age	days	135.9 ± 18.8	110 ± 3.96	142.7 ± 16.1	0.2196	0.306	0.92
Weight	g	31.15 ± 2.16	30.4 ± 1.79	29.9 ± 1.64	0.9023	0.941	0.866

GI motility monitor ANOVA and Dunnett post-test summary. Mean values and SEMs are shown. N: number of mice (and ilea) analyzed with the GIMM. Grey-colored boxes highlight significant p-values (<0.05). Weight and age were not significantly different among genotypes.

Supplementary References

1. Shesely EG, *et al.* (1996) Elevated blood pressures in mice lacking endothelial nitric oxide synthase. *Proc Natl Acad Sci U S A* 93(23):13176-13181.
2. Brenman JE, *et al.* (1996) Interaction of Nitric Oxide Synthase with the Postsynaptic Density Protein PSD-95 and α1-Syntrophin Mediated by PDZ Domains. *Cell* 84(5):757-767.
3. Huang PL, Dawson TM, Bredt DS, Snyder SH, & Fishman MC (1993) Targeted disruption of the neuronal nitric oxide synthase gene. *Cell* 75(7):1273-1286.
4. Nagy A, Gertsenstein M, Vintersten K, & Behringer R (2008) Karyotyping Mouse Cells. *CSH Protoc* 2008(5):pdb.prot4706.
5. Hurt KJ, *et al.* (2012) Cyclic AMP-dependent phosphorylation of neuronal nitric oxide synthase mediates penile erection. *Proc Natl Acad Sci U S A* 109(41):16624-16629.
6. Gilda JE & Gomes AV (2013) Stain-Free total protein staining is a superior loading control to beta-actin for Western blots. *Anal Biochem* 440(2):186-188.
7. Moritz CP (2017) Tubulin or Not Tubulin: Heading Toward Total Protein Staining as Loading Control in Western Blots. *PROTEOMICS* 17(20):1600189.
8. Duan L-P, Wang HH, & Wang DQ-H (2004) Cholesterol absorption is mainly regulated by the jejunal and ileal ATP-binding cassette sterol efflux transporters Abcg5 and Abcg8 in mice. *J Lipid Res* 45(7):1312-1323.
9. Curro D, Volpe AR, & Preziosi P (1996) Nitric oxide synthase activity and non-adrenergic non-cholinergic relaxation in the rat gastric fundus. *Br J Pharmacol* 117(4):717-723.
10. Shuttleworth CW, Sanders KM, & Keef KD (1993) Inhibition of nitric oxide synthesis reveals non-cholinergic excitatory neurotransmission in the canine proximal colon. *Br J Pharmacol* 109(3):739-747.
11. Linden A, Ullman A, Skoogh BE, & Lofdahl CG (1992) The non-adrenergic, non-cholinergic response counteracts changes in guinea-pig airway tone with and without sympathetic activation. *Br J Pharmacol* 106(3):616-622.
12. Pinna C, Bolego C, & Puglisi L (1995) Effect of substance P and capsaicin on stomach fundus and ileum of streptozotocin-diabetic rats. *Eur J Pharmacol* 276(1-2):61-69.
13. Denisova OV, *et al.* (2014) Akt Inhibitor MK2206 Prevents Influenza pH1N1 Virus Infection In Vitro. *Antimicrob Agents Chemother* 58(7):3689-3696.
14. Leemhuis J, Boutillier S, Schmidt G, & Meyer DK (2002) The Protein Kinase A Inhibitor H89 Acts on Cell Morphology by Inhibiting Rho Kinase. *J Pharmacol Exp Ther* 300(3):1000-1007.
15. Kaya AI, *et al.* (2012) Cell Contact-dependent Functional Selectivity of β(2)-Adrenergic Receptor Ligands in Stimulating cAMP Accumulation and Extracellular Signal-regulated Kinase Phosphorylation. *J Biol Chem* 287(9):6362-6374.
16. Satin J, *et al.* (2004) Mechanism of spontaneous excitability in human embryonic stem cell derived cardiomyocytes. *J Physiol* 559(Pt 2):479-496.
17. Chen X, Feng L, & Jin H (2013) Constant or fluctuating hyperglycemias increases cytomembrane stiffness of human umbilical vein endothelial cells in culture: roles of cytoskeletal rearrangement and nitric oxide synthesis. *BMC Cell Biol* 14(1):22.
18. Garvey EP, *et al.* (1997) 1400W Is a Slow, Tight Binding, and Highly Selective Inhibitor of Inducible Nitric-oxide Synthase in Vitro and in Vivo. *J Biol Chem* 272(8):4959-4963.
19. Monks J, *et al.* (2016) Xanthine oxidoreductase mediates membrane docking of milk- fat droplets but is not essential for apocrine lipid secretion. *J Physiol* 594(20):5899-5921.
20. Belkind-Gerson J, *et al.* (2017) Colitis promotes neuronal differentiation of Sox2+ and PLP1+ enteric cells. *Sci Rep* 7(1):2525.
21. Smith TH, Ngwainmbi J, Grider JR, Dewey WL, & Akbarali HI (2013) An In-vitro Preparation of Isolated Enteric Neurons and Glia from the Myenteric Plexus of the Adult Mouse. *J Vis Exp* (78):10.3791/50688.

22. Hoffman JM, Brooks EM, & Mawe GM (2010) Gastrointestinal Motility Monitor (GIMM). *J Vis Exp* (46).
23. Wong KKL, Tang LCY, Zhou J, & Ho V (2017) Analysis of spatiotemporal pattern and quantification of gastrointestinal slow waves caused by anticholinergic drugs. *Organogenesis* 13(2):39-62.
24. McGill M, Klinger-Lawrence M, & Herrera G (2016) Disruption of Serotonin Signaling Results in Loss of Coordinated Tone Development and Subsequent Inhibition of Peristalsis in Guinea Pig Distal Colon. *FASEB J* 30(1_supplement):1254.1256-1254.1256.
25. Sarna SK & Otterson MF (1988) Gastrointestinal Motility: Some Basic Concepts. *Pharmacology* 36(suppl 1)(Suppl. 1):7-14.
26. Janssen PW, *et al.* (2007) Characterization of flow and mixing regimes within the ileum of the brushtail possum using residence time distribution analysis with simultaneous spatio-temporal mapping. *J Physiol* 582(Pt 3):1239-1248.
27. Kendig DM, Hurst NR, & Grider JR (2016) Spatiotemporal Mapping of Motility in Ex Vivo Preparations of the Intestines. *J Vis Exp* (107):53263.